This is the pre-peer reviewed version of the following article: Spratte, T., Geiger, S., Colombo, F., Mishra, A., Taale, M., Hsu, L.-Y., Blasco, E., Selhuber-Unkel, C., Increasing the Efficiency of Thermoresponsive Actuation at the Microscale by Direct Laser Writing of pNIPAM. *Adv. Mater. Technol*. 2022, 2200714., which has been published in final form at https://doi.org/10.1002/admt.202200714. This article may be used for non-commercial purposes in accordance with Wiley Terms and Conditions for Use of Self-Archived Versions.

Increasing the Efficiency of Thermoresponsive Actuation at the Microscale by Direct Laser Writing of pNIPAM

*Tobias Spratte, Sophie Geiger, Federico Colombo, Ankit Mishra, Mohammadreza Taale, Li-Yun Hsu, Eva Blasco, Christine Selhuber-Unkel**

T. Spratte, S. Geiger, Dr. F. Colombo, A. Mishra, Dr. M. Taale, Prof. C. Selhuber-Unkel
Institute for Molecular Systems Engineering (IMSE), Heidelberg University, 69120 Heidelberg, Germany
E-Mail: selhuber@uni-heidelberg.de

L.-Y. Hsu, Prof. Dr. E. Blasco
Organic Chemistry Institute and Center for Advanced Materials, Heidelberg University, 69120 Heidelberg, Germany

Keywords: soft microactuators, direct laser writing, two-photon-polymerization, responsive materials, thermoresponsive hydrogels

Abstract

Thermoresponsive hydrogels such as poly(*N*-isopropylacrylamide) (pNIPAM) are highly interesting materials for generating soft actuator systems. Whereas the material has so far mostly been used in macroscopic systems, we here demonstrate that pNIPAM is an excellent material for generating actuator systems at the micrometer scale. Two-Photon Direct Laser Writing was used to precisely structure thermoresponsive pNIPAM hydrogels at the micrometer scale based on a photosensitive resist. We systematically show that the surface-to-volume ratio of the microactuators is decisive to their actuation efficiency. The phase

transition of the pNIPAM was also demonstrated by nanoindentation experiments. We observed that the mechanical properties of the material can easily be adjusted by the writing process. Finally, we found that not only the total size and surface structure of the microactuator plays an important role, but also the crosslinking of the polymer itself. Our results demonstrate for the first time a systematic study of pNIPAM-based microactuators, which can easily be extended to systems of microactuators that act cooperatively, e.g., in microvalves.

1. Introduction

Active materials for stimuli-controlled microactuation can strongly improve the function of many applications related to lab-on-a-chip devices, from the manipulation of single cells to controlling microfluidic systems.[1],[2],[3],[4] Due to its thermoresponsive properties, poly(*N*-isopropylacrylamide) (pNIPAM) is an excellent material for generating actuators in aqueous environments. [5],[6],[7] The thermoresponsive properties of pNIPAM are based on a reversible phase transition at the lower critical solvent temperature (LCST) due to a globule-to-coil transition.[8] Below the LCST the polymer is in a hydrophilic, hydrated state, while above the LCST it is in a hydrophobic state. In this state, the interactions of the polymer with itself lead to a higher gain in free energy than would be achieved by solvation energy. The volume of pNIPAM materials in the hydrated, swollen state is much higher than in the hydrophobic state, because water is integrated into the material in the hydrated state.[9] As the actuation of pNIPAM hydrogel is based on its water-dependent shrinkage and swelling, the actuation efficiency and the forces generated by pNIPAM-based actuators critically depend on the in- and outflow of water through the pores of the material. Therefore, the actuation effect, including actuation dynamics as well as stroke forces, can be improved by introducing pores into the material.[10],[11]

Whereas in previous studies template-assisted methods have proven highly suitable for introducing pores into hydrogels, they lack local microstructural control, while being excellent for structuring macroscopic samples with an interconnected structure.[10] For generating highly efficient pNIPAM-based microactuators, a precisely defined design is required and thus methods are needed that allow for their highly precise 3D structuring at the micrometer scale.

The technology of additive nano- and micromanufacturing opens doors to novel and remarkable microengineering possibilities and even enables printing of simple three-dimensional volumetric structures at small scales.[12] Direct Laser Writing (DLW) involving two-photon-polymerization of photoresists is one of the additive manufacturing techniques that can be used to fabricate intricate and miniaturized three-dimensional structures, as they are required for the fabrication of microactuators. By utilizing two-photon-absorption and a femtosecond pulsed laser, this fabrication method allows to print in sub-micrometer resolution, even with several materials and on different types of substrates.[13],[14] Direct Laser Writing has also proven highly suitable for fabricating 4D materials, i.e. responsive materials that change their properties due to an external stimulus.[15] For example, the shape of such materials could be controlled at the micrometer scale by temperature and light.[16]

Here we report a novel strategy for generating precisely designed pNIPAM-based microactuator systems through DLW and to systematically investigate their shrinkage and swelling properties in detail. In particular, we focus on studying the influence of microactuator size and different actuator designs, as well as DLW parameters, on the total actuation of the material. The so generated microactuators permit directional and temperature-controlled actuation and have a great perspective for application in microactuator systems, e.g., to control microvalves or microbrushes.

2. Results and Discussion

Thermoresponsive pNIPAM hydrogel microstructures were fabricated by a high-precision Direct Laser Writing (DLW) approach.[17] In brief, a photo-sensitive resist containing *N*-isopropylacrylamide monomers, *N*,*N*'-methylenebis(acrylamide) comonomers and lithium phenyl(2,4,6-trimethylbenzoyl)phosphinate (LAP) photoinitiator is produced according to the work of Hippler et al., which can be polymerized by two-photon-absorption.[16] A focused femtosecond pulsed near infrared (NIR) laser (λ=780 nm) is used to initiate the polymerization in a very small volume (< 1 μm^3). **Figure 1a** describes the fabrication process schematically, in which a droplet of the pNIPAM resist is cast onto a glass substrate and the focused laser is scanned in lines and slices to write the hydrogel microstructures based on a computer design. Different pillar designs are depicted in **Figure 1b**, including cylinders, hollow cylinders and star shaped pillars. In addition, 3D reconstructions of confocal fluorescence image stacks of the

fabricated microstructures are presented, which demonstrate the success of the DLW process. To reduce shrinking restraints of the micropillars at the hydrogel/glass interface, the structural design contains a small pedestal at the bottom of the pillars, which links the hydrogel to the substrate.

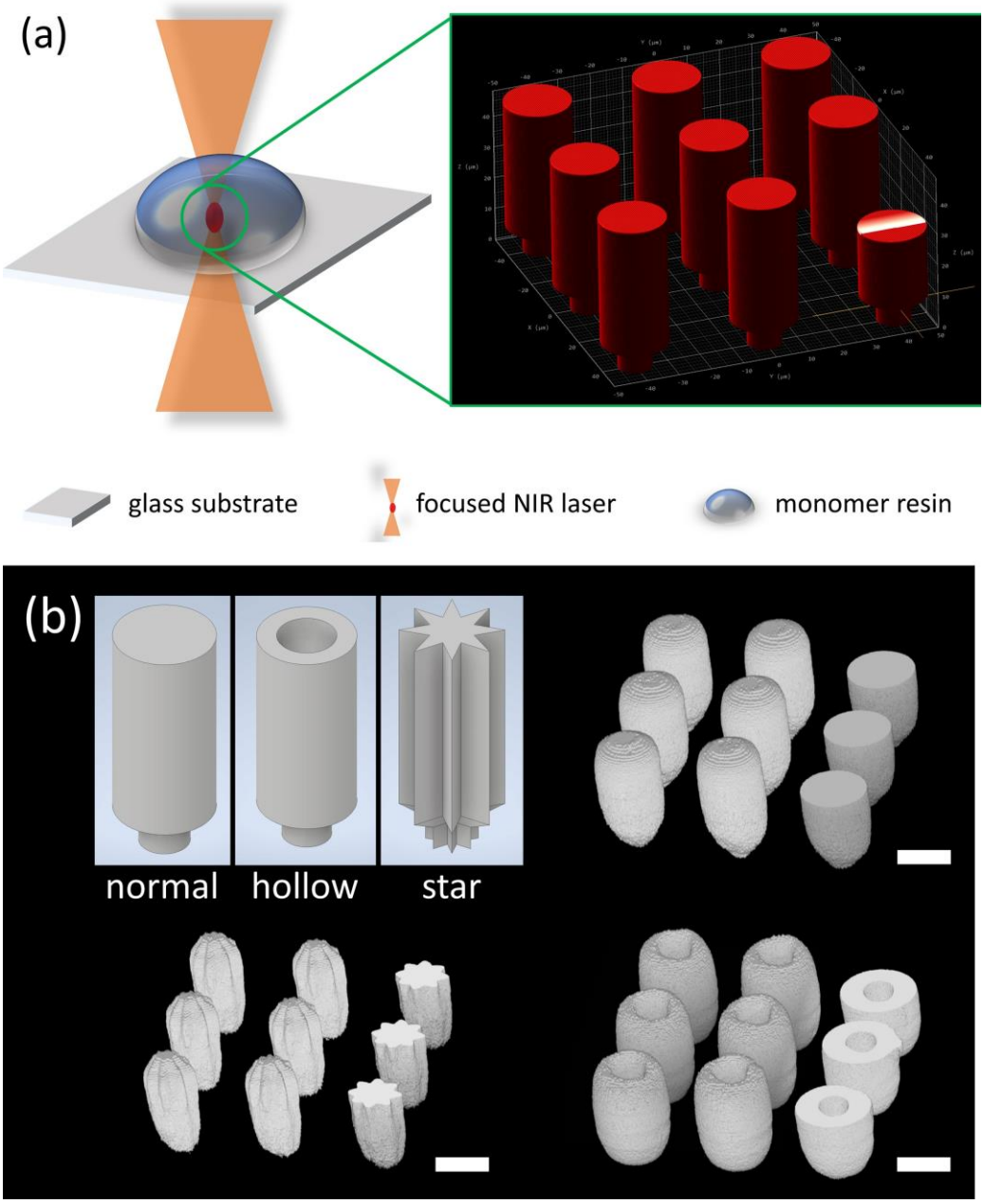

Figure 1. Direct Laser Writing of pNIPAM microactuators. (a) The DLW fabrication process is depicted schematically. A pulsed and highly focused NIR laser (λ=780 nm, t_{pulse}=100 fs) is used to initiate two-photon-polymerization (2PP) of a monomer resin in a very locally confined volume. By scanning the laser both in lateral directions (XY) and in different slices (Z), it is possible to fabricate 3D microstructures based on a computer model. (b) Models of different

architectures constructed via computer aided design (CAD) are shown (top left) as well as 3D reconstructions of measured confocal fluorescence image stacks of the fabricated structures, each including a system of nine pNIPAM microactuators. On purpose, the three images to the right in each actuator system show the cross-section of the actuators. These images prove the applicability of the DLW fabrication process to yield the desired hydrogel microstructures. Scale bars are 20 µm.

Various sizes and architectures of pNIPAM micropillars were fabricated to investigate the effect of surface-to-volume ratio on the shrinking and swelling properties of the hydrogel microstructures. In a previous work we have demonstrated that structuring pNIPAM at the microscale by introducing an interconnected network of microchannels can drastically enhance the in- and outflow of water and hence the responsivity of the hydrogel even in bulk samples.[10] As DLW allows for a high freedom in 3D design, several material properties were analyzed to study the performance of the microactuators prepared by DLW in this work.

First, the thermoresponsive shrinking and swelling properties of the material were investigated by fluorescence confocal imaging of the pNIPAM microstructures at different temperatures. These results are summarized in **Figure 2**, where a 2D comparison of cross-sections and a 3D comparison of volumes of the hydrogel structures before and after shrinking at 22 °C and 45 °C, respectively are presented. In a first experiment, cylindrical micropillars of various sizes (aspect ratio 2:1, height:diameter) were analyzed, where the cross-section areas in the center of each pillar and the volumes were measured at 22 °C and 45 °C (**Figure 2a**). The percentual shrinkage of each microstructure was calculated according to **Equation 1** for the 2D case and **Equation 2** for the 3D case, where *A* and *V* refer to the cross-section areas and volumes at a specific temperature, respectively.

$$Shrinkage_{2D} = 1 - \frac{A_{45°C}}{A_{22°C}} \times 100\% \quad (1)$$

$$Shrinkage_{3D} = 1 - \frac{V_{45°C}}{V_{22°C}} \times 100\% \quad (2)$$

In a second experiment, different architectures of microstructures of the same size were evaluated in the same manner (**Figure 2b**). Finally, the percentual shrinkage is presented as a function of perimeter-to-cross-section ratio (2D) and surface-to-volume ratio (3D) in **Figure 2c and d**, respectively.

From these results a significant increase in shrinkage can be observed as the microstructure dimensions get smaller. Whereas the 50 µm diameter pillar shrinks very little, the 10 µm diameter pillar reduces its volume by 41 +/- 3 %. A similar trend is observed for the different architectures of micropillars, where the shrinkage increases with larger surface-to-volume ratio. The increase in shrinkage can be related to a facilitated outflow of water from the microstructure, the thinner the sample dimensions get.[18] This means controlling the shape of the microstructures by the fabrication process can drastically improve the actuation capabilities.

To investigate the reversibility of shrinking and swelling, the microstructures were cooled down to 22 °C after the initial shrinking at 45 °C, and the sample dimensions were evaluated again. These results are depicted in **Figure S1** and prove, that the initial dimensions can be restored after cooling, which is in agreement to previous results on pNIPAM microgels in surface coatings.[9]

In addition to the temperature-induced volume change, also the mechanical properties of the pNIPAM hydrogel change during the material's phase transition, as they mainly depend on the degree of hydration. The intrinsic mechanical properties of the hydrogel at constant temperature are especially important for the use in soft microactuators, where commonly mechanical work is generated by a volume change. The material stiffness strongly depends on the degree of crosslinking and is reduced for a lower degree, while stiffness increases with a higher crosslinking degree.[19] Therefore, pNIPAM microstructures fabricated by different writing speeds and fixed laser power were studied in nanoindentation experiments. For the DLW process used in this work, the degree of crosslinking increases with higher doses of laser light initiating the polymerization. A higher dose will result in a polymer network exhibiting a higher crosslinking density and therefore different material properties, despite using the same resin. The exact crosslinking degree in the final microstructures remains unknown though. A comparison of writing speed, relative crosslink density and shrinkage can be found in the supporting information in **Figure S2**, which concludes that higher writing speeds result in higher shrinkage and eventually less crosslinking. These findings agree with other studies in this field.[20]

Figure 3a depicts the nanoindentation process schematically, where a cantilever with spherical tip is used to indent into the surface of pNIPAM microcubes at several locations. A microscope image showing an array of identical test structures and the cantilever is displayed

in **Figure 3b**. Representative load-indentation curves of microstructures fabricated with a writing speed of 30 mm/s are presented in **Figure 3c and d** for 22 °C and 45 °C, respectively. From these plots a significant change in surface stiffness is observed before and after the phase transition of pNIPAM microcubes, a 3D structure specifically chosen for the indentation tests. For a moderate writing speed of 30 mm/s the effective Young's modulus increases from 19 +/- 5 kPa at 22 °C to 475 +/- 74 kPa at 45 °C. This increase in stiffness is related to the dehydration of the hydrogel above 32 °C, in which water is flowing out of the material and the polymer network densifies.[21] The results are in compliance with Schmidt et al., who investigated the mechanical properties of pNIPAM microgel films and observed a transition in elastic modulus from less than 100 kPa at 25 °C to above 600 kPa at 47 °C.[22]

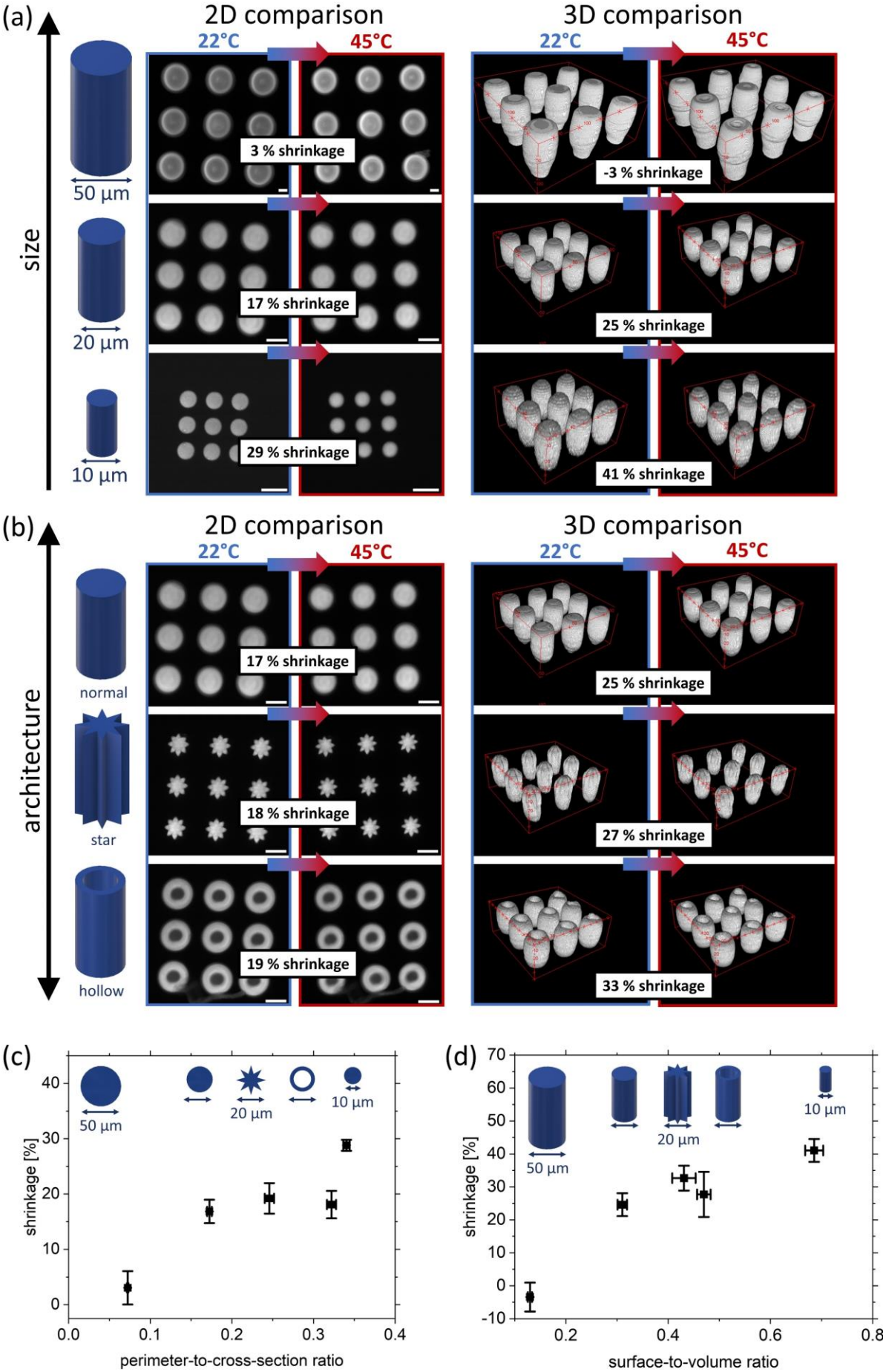
(a)
2D comparison
3D comparison
22°C
45°C
size
50 µm
20 µm
10 µm
3 % shrinkage
17 % shrinkage
29 % shrinkage
-3 % shrinkage
25 % shrinkage
41 % shrinkage
(b)
architecture
normal
star
hollow
17 % shrinkage
18 % shrinkage
19 % shrinkage
25 % shrinkage
27 % shrinkage
33 % shrinkage
(c)
shrinkage [%]
perimeter-to-cross-section ratio
(d)
surface-to-volume ratio

1

Figure 2. Thermally induced shrinkage of pNIPAM hydrogel microstructures for different micropillar sizes (a) and architectures (b). A comparison of all hydrogel structures is illustrated by confocal fluorescence images of cross-sections and 3D reconstructions of the image stacks. Scale bars are 20 µm. In both cases the shrinkage increases with increasing surface-to-volume ratio (3D) and perimeter-to-cross-section ratio (2D), respectively. This is explained by the ease of water flowing out of the hydrogel for larger surfaces. (c) and (d) summarize these findings in plots, where a clear trend of increased shrinkage is observed. Error bars denote standard deviations calculated from nine tested samples each.

Furthermore, a relation between writing speed and material stiffness is observed. Increasing the writing speed results in a decreased surface stiffness, both for 22 °C and 45 °C. This can be explained by a lower dose of laser light for higher writing speeds, which provides less energy to initiate polymerization and thus results in fewer crosslinks. The direct relation between writing speed and material stiffness allows to simply control the mechanical properties of the microstructures and thus highlights the great potential of DLW as a fabrication technology for soft microactuators.[23]

For the polymer resist used in this work, a range of writing speeds from 10 mm s^{-1} to 50 mm s^{-1} was suitable. Slower writing speeds resulted in microexplosions due to excessive energy input, while faster writing speeds did not cause polymerization at all. However, these limits can also be influenced by other writing parameters, such as laser power, hatching and slicing distances, and the chemical composition of the resist. Altogether these factors offer many degrees of freedom to adjust the material properties and highlight the versatile utilization of the DLW technology presented in this work.

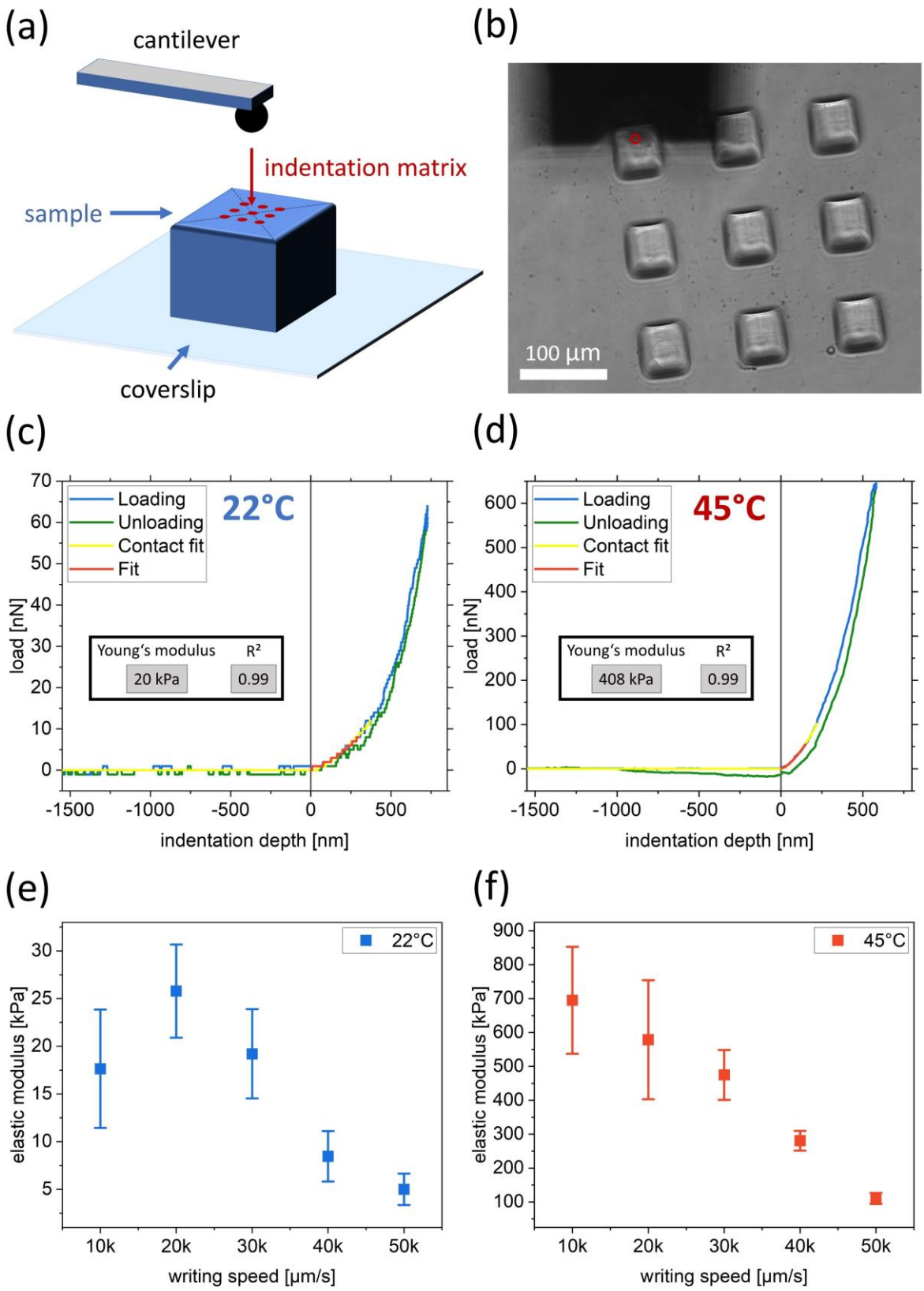

Figure 3. Mechanical characterization of the material as a function of temperature and writing speed. (a) A schematic of the microindentation experiment is depicted. Indentations at several locations on the hydrogel microstructures were performed using a cantilever with

spherical tip. (b) A microscope image during an indentation experiment shows the cube shaped hydrogel microstructures and the cantilever with indicated tip (red circle). Representative load-indentation-curves including Hertz fits and corresponding effective Young's modulus values are presented for (c) 22 °C and (d) 45 °C. A comparison of the stiffness of hydrogel microstructures printed at various writing speeds is shown both for (e) 22 °C and (f) 45 °C. The stiffness of all tested samples is higher at 45 °C compared to 22 °C, which is due to the thermoresponsive properties of pNIPAM hydrogels. For both temperatures a trend of decreasing stiffness with increasing writing speed is observed. Error bars denote standard deviations calculated from 27 indentations each.

To demonstrate the actuation capabilities and design freedom of the actuators fabricated with our DLW technology, two examples of soft microactuator systems were designed. First, temperature controlled microvalves were fabricated, which are depicted in **Figure 4a**. The valves have a diameter of 60 µm and consist of a ring-shaped base with a circular lid on top. The lid is made of several triangular sections arranged in circular fashion such that one end of each section points in the valve center to create a round opening. The base is fabricated with a low writing speed and thus shrinks less, while for the lid a high writing speed is used, which results in a significant shrinkage. Therefore, the opening of the microvalves becomes larger upon heating and smaller upon cooling (cf. dashed red circle). Furthermore, the magnitude of shrinkage and opening increases with higher writing speeds, which is related to a less crosslinked polymer network for high writing speeds. This observation confirms the previously mentioned benefit of the DLW technology to adjust the material properties easily by, e.g., varying the writing speed *in situ*. The microvalve structures shown here can find application in capturing and release of microobjects, microparticles and bioactive cargos like cells or bacteria.

Another possible application is presented in **Figure 4b**, which illustrates a system of pNIPAM micropillars that can be actuated by temperature. Here, a square array of 100 micropillars is heated to 50 °C to induce a shrinkage and a change in gap size between the pillars. This temperature-controlled variation in gap size could be utilized to design a dynamic hydrogel brush for cell sorting applications, having the potential to tremendously increase the flexibility of the current non-dynamic lab-on-a-chip sorting devices.[24]

For all microstructures presented in this work, the actuation speed was limited by the heating and cooling rates of the microscope chambers, which was in the range of minutes, rather than the hydrogel material itself. We believe that the microstructures adapt to the environment much faster due to their high surface-to-volume ratios compared to larger bulk samples. Other studies found that such structures can even be actuated within the millisecond range, via locally heating with a laser beam.[16] These fast actuation capabilities are essential factors for the application range of the responsive material.

In addition to these two examples of microactuators, various other designs could be realized with high precision and high flexibility of adjusting material properties by the DLW process presented. Therefore, this approach of engineering responsive soft microactuators with improved actuation capabilities offers great potential for other fields of manufacturing soft microrobotic devices, or even humidity sensing.[25],[26],[27]

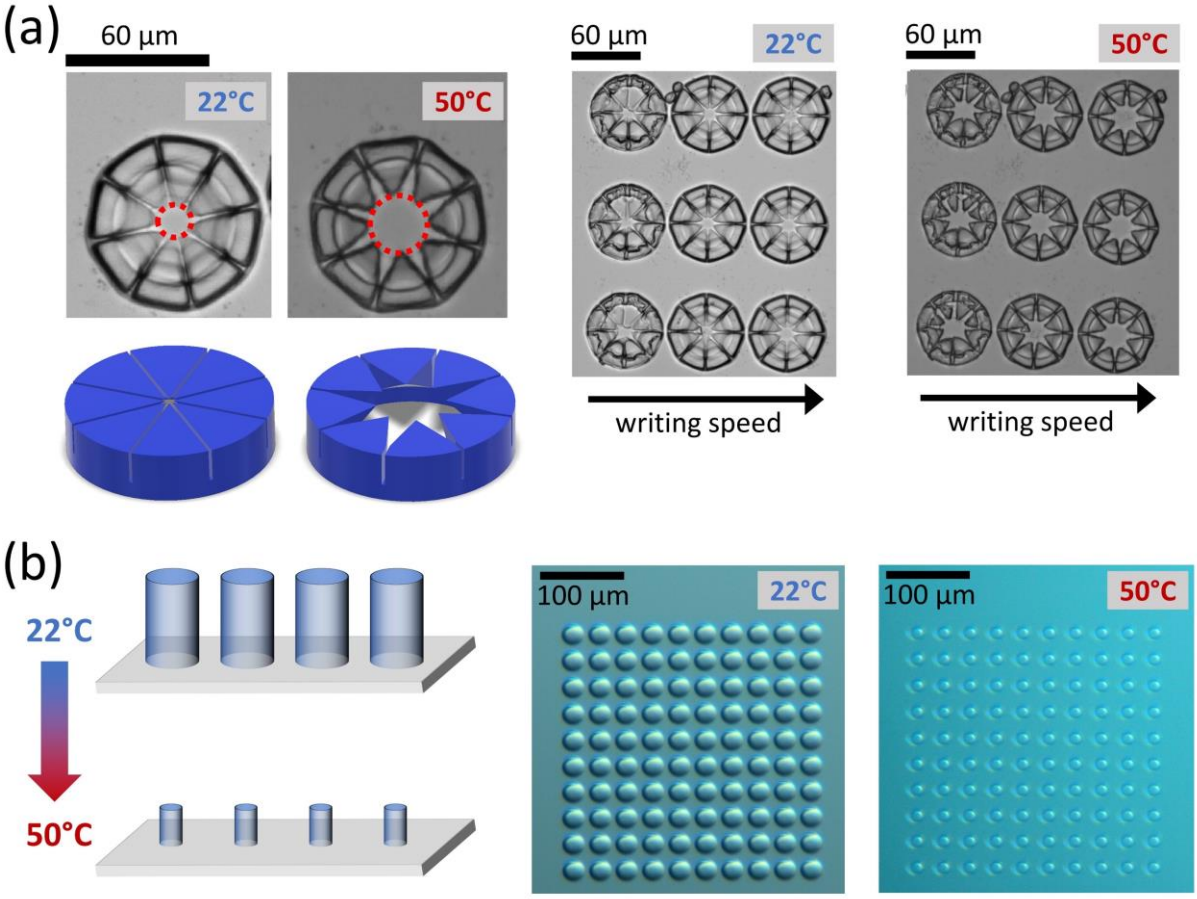

Figure 4. Thermoresponsive pNIPAM microactuators are presented. (a) Bright field images of pNIPAM hydrogel microvalves. The valves open during heating from 22 °C to 50 °C and demonstrate the working principle of a possible application of DLW fabricated stimuli

responsive soft microactuators. The magnitude of shrinkage and opening increases with higher writing speeds. (b) Sketch and microscopy images of a 10 by 10 array of cylindrical pNIPAM micropillars (d=10 µm, h=20 µm), which are swollen at 22 °C and shrunken at 50 °C. The gap size between the micropillars changes as a function of temperature and thus these structures could find application in sorting devices, similar to a dynamic brush.

3. Conclusion

This work paves the way towards the precise fabrication of micrometer sized actuator systems by a robust method based on DLW. Our results emphasize that pNIPAM is a promising material for printing micrometer-sized actuating objects. The dependency of actuation efficiency on the size and design of the printed microobjects suggests the surface-to-volume ratio of the object is a critical parameter for efficient microactuation function. To this end we propose that DLW is a great technology to prepare pNIPAM based microactuators not only as single microactuators, but even microactuator systems. The ability to assemble microactuators with micrometer resolution in almost arbitrary 3D shapes and to position them at a defined place on a surface may find a wide range of applications in future microrobotic systems that are based on thermoresponsive materials.

4. Experimental Section

Materials:

N-isopropylacrylamide (Sigma-Aldrich, ≥99%), *N*,*N*'-methylenebis(acrylamide) (Sigma-Aldrich, >99%), lithium phenyl(2,4,6-trimethylbenzoyl)phosphinate (Sigma-Aldrich, ≥95%), ethylene glycol (Sigma- Aldrich, ≥99%), acryloxyethyl thiocarbamoyl Rhodamine B (Polysciences), 3-(trimethoxysilyl)propyl methacrylate (Sigma-Aldrich, 92%), ethanol (99%). All chemicals were used without further purification.

pNIPAM-Resist formulation:

The resist formulation has been adapted from Hippler et al.[16] For the preparation of the pNIPAM-resist 400 mg *N*-isopropylacrylamide, 40 mg *N*,*N*'-methylenebis(acrylamide) and 10

mg lithium phenyl(2,4,6-trimethylbenzoyl)phosphinate were dissolved in 450 µL of ethylene glycol at room temperature and under constant magnetic stirring. To label the material for fluorescence imaging, 4 mg of acryloxyethyl thiocarbamoyl Rhodamine B was added. The solution was kept in dark to protect the photosensitive compounds from light.

Fabrication of pNIPAM hydrogel microstructures:

3D microstructures of pNIPAM hydrogel were fabricated with a commercially available Direct Laser Writing setup (Photonic Professional GT2, Nanoscribe GmbH & Co. KG) using oil immersion configuration with a 25 ×, NA= 0.8 immersion objective. All microstructures were fabricated with 100% laser power (power scale=1), slicing distance of 0.3 µm and hatching distance of 0.2 µm. The laser scanning speed was varied between 10 mm s^{-1} and 50 mm s^{-1} to yield microstructures with different degrees of crosslinking. After writing, the microstructures were developed in 40 ml deionized water for 10 minutes and subsequently transferred into a fresh beaker of 40 ml deionized water for 1 minute. The samples were kept in deionized water at 22 °C for storage. To facilitate adhesion of the microstructures to the glass substrates (borosilicate glass, 130-160 µm thickness), coverslips were functionalized with 3-(trimethoxysilyl)propyl methacrylate: First, the coverslips were cleaned in MilliQ water under sonication for 5 minutes and subsequently sonicated for another 5 minutes in ethanol. The substrates were dried with a heat gun and incubated in 3-(trimethoxysilyl)propyl methacrylate (15 mM in ethanol). After rinsing with MilliQ water and ethanol the substrates were dried with a heat gun and kept in an oven at 80 °C for 2 hours.

Computer models of the sample geometries were designed with *Autodesk Inventor Professional 2019* and imported as stl-files into the slicing software *Describe*, which defines the writing parameters.

Confocal Imaging:

A laser scanning fluorescent microscope (Nikon A1R, Nikon Imaging Center Heidelberg) was used to study the sample response to temperature. The acquisition of the images was performed with a Nikon Plan Fluor 40x NA 1.3 objective. The glass coverslip with the sample was analyzed at room temperature and, after acclimatizing the sample for 15 minutes, in a temperature-controlled chamber (Tokai Hit chamber). The chamber temperature was regulated by an external controller (STXG Tokai controller) that was set up as following: top

heater 65 °C, bath heater 50 °C, stage heater 50 °C, sample temperature 40 °C. The sample was always kept hydrated using ultrapure water filtered 0.22 µm.

Confocal fluorescence images were analyzed with *ImageJ*. First, an intensity threshold was defined and applied to all samples to create binary images. These binary images were then processed using binary operations *Erode*, *Dilate*, *Open* and *Close*. For the 2D images a cross-section of the micropillars was chosen and using the *measure particle* function the area and the perimeter were analyzed. For the 3D images the ImageJ Plugin '*3D objects counter*' was used to evaluate surface area and volume.[28]

Micromechanical characterization:

To quantify the mechanical properties of the printed materials, nanoindentations at the microstructure surfaces were performed with a commercially available fiber-optics based nanoindenter (Pavone, *Optics11*, Netherlands). For this purpose, pNIPAM microcubes with a side length of 50 µm were fabricated in square arrays of 3 by 3 cubes (cf. **Figure 3b**). Five arrays were fabricated with various laser scanning speeds ranging from 10 mm s^{-1} to 50 mm s^{-1} in steps of 10 mm s^{-1}. A pre-calibrated indenter probe with a cantilever spring constant of k=0.23 N m^{-1} and a spherical glass tip of 3 µm radius was used for all experiments. For all arrays three cubes were tested in a matrix scan manner, which means that for each cube a square matrix of 3 by 3 indentation points with a lateral distance of 2 µm from each other was chosen in the center of each cube (cf. **Figure 3a**). For each location an indentation profile of 500 nm indentation at a speed of 1 µm s^{-1} followed by a hold time of 0.5 s and subsequent retraction at 1 µm s^{-1} was applied. The samples were immersed in deionized water throughout all experiments and equilibrated for at least 24 hours before the measurements. Load-indentation curves were recorded both at 22 °C and 45 °C by using the internal temperature-controlled chamber of the device.

Data analysis was done using the *Data Viewer* (V2.5.0) software supplied by the device manufacturer. To determine the Young's modulus from each load-indentation curve, Hertzian contact model was applied according to a publication of Huth et al., using a constant indentation speed.[29] The contact point of each load-indentation curve was found by using the software integrated contact fit up to 20% of the maximum load. The Hertz fits were applied in the range between contact point (0 nm) and 300 nm for 22 °C or 0 nm and 150 nm for 45 °C, respectively.

Supporting Information

Supporting Information is available from the Wiley Online Library or from the author.

Acknowledgements

T.S. and C.S. thank the German Research Foundation for funding through the project SE 1801/4-1 within the Priority Programme SPP 2206 “KOMMMA”. S. G., F. C. and C. S. acknowledge the European Research Council through the Consolidator Grant PHOTOMECH (no. 101001797). We also thank the German Research Foundation for funding through the RTG 2154. C.S. was supported through the Max Planck School Matter to Life supported by the German Federal Ministry of Education and Research (BMBF) and the Flagship Initiative “Engineering Molecular Systems”. E.B. and C.S. also acknowledge funding by the DFG under Germany’s Excellence Strategy 2082/1-390761711 (3D Matter Made to Order) and the Carl Zeiss Foundation. The authors would like to thank the Nikon Imaging Center in Heidelberg for their support.

Received: ((will be filled in by the editorial staff))
Revised: ((will be filled in by the editorial staff))
Published online: ((will be filled in by the editorial staff))

References

[1] J. Kim, J. W. Kim, H. C. Kim, L. Zhai, H. U. Ko, R. M. Muthoka, *Int. J. Precis. Eng. Manuf.* **2019**, *20*, 2221.

[2] Y. Yamanishi, S. Sakuma, F. Arai, *Proc. - IEEE Int. Conf. Robot. Autom.* **2008**, 899.

[3] J. H. Jung, C. Han, S. A. Lee, J. Kim, C. Yang, *Lab Chip.* **2014**, *14*, 3781.

[4] L. F. Kadem, K. G. Suana, M. Holz, W. Wang, H. Westerhaus, R. Herges, C. Selhuber-Unkel, *Angew. Chem. Int. Ed*. **2017**, *56*, 225.

[5] A. Halperin, M. Kröger, F. M. Winnik, *Angew. Chem. Int. Ed.* **2015**, *54*, 15342.

[6] J. Liu, L. Jiang, S. He, J. Zhang, W. Shao, *Chem. Eng.* **2022**, *433*, 133496.

[7] A. Sutton, T. Shirman, J. Timonen, G. T. England, P. Kim, M. Kolle, T. Ferrante, L. D. Zarzar, E. Strong, J. Aizenberg, *Nat. Commun*. **2017**, *8*, 14700.

[8] C. Wu, X. Wang, *Phys. Rev. Lett*. **1998**, *80*, 4092.

[9] S. Schmidt, H. Motschmann, T. Hellweg, R. von Klitzing, *Polym*. **2008**, *49*, 749.

[10] T. Spratte, C. Arndt, I. Wacker, M. Hauck, R. Adelung, R. R. Schröder, F. Schütt, C. Selhuber-Unkel, *Adv. Intell. Syst.*, **2022**, *4,* 2100081.

[11] J. T. Zhang, R. Bhat, K. D. Jandt, *Acta Biomater*. **2009**, *5*, 488.

[12] M. Vaezi, H. Seitz, S. Yang, *Int. J. Adv. Manuf. Technol.* **2013***, 67*, 1721.

[13] C. Barner-Kowollik, M. Bastmeyer, E. Blasco, G. Delaittre, P. Müller, B. Richter, M. Wegener, *Angew. Chem. Int. Ed*. **2017**, *56*, 15828.

[14] T. Gissibl, S. Thiele, A. Herkommer, H. Giessen, *Nat. Photon*. **2016**, *10*, 554.

[15] C. A. Spiegel, M. Hippler, A. Münchinger, M. Bastmeyer, C. Barner-Kowollik, M. Wegener, E. Blasco, *Adv. Funct. Mater*. **2020**, *30*, 1907615.

[16] M. Hippler, E. Blasco, J. Qu, M. Tanaka, C. Barner-Kowollik, M. Wegener, M. Bastmeyer, *Nat. Commun.* **2019***, 10*, 232.

[17] S. Maruo, O. Nakamura, S. Kawata, *Opt. Lett*. **1997**, *22*, 132.

[18] K. Depa, A. Strachota, M. Šlouf, J. Hromádková, *Eur. Polym. J*. **2012**, *48*, 1997.

[19] A. Burmistrova, M. Richter, C. Uzum, R. V. Klitzing, *Colloid Polym. Sci*. **2011**, *289*, 613.

[20] R. Contreras-Cáceres, L. Schellkopf, C. Fernández-López, I. Pastoriza-Santos, J. Pérez-Juste, M. Stamm, *Langmuir*. **2015**, *31*, 1142.

[21] M. A. Haq, Y. Su, D. Wang, *Mater. Sci. Eng. C*. **2017**, *70*, 842.

[22] S. Schmidt, M. Zeiser, T. Hellweg, C. Duschl, A. Fery, H. Möhwald, *Adv. Funct. Mater*. **2021**, *20*, 3235.

[23] E. Sedghamiz, M. Liu, W. Wenzel, *Nat. Commun*. **2022**, *13*, 2115.

[24] J. P. Beech, S. H. Holm, K. Adolfsson, J. O. Tegenfeldt, *Lab Chip*. **2012**, *12*, 1048.

[25] Z. Lao, N. Xia, S. Wang, T. Xu, X. Wu, L. Zhang, *Micromachines.* **2021**, *12*, 465.

[26] F. Muralter, F. Greco, A. M. Coclite, *ACS Appl. Polym. Mater*. **2020**, *2*, 1160.

[27] C. Dingler, H. Müller, M. Wieland, D. Fauser, H. Steeb, S. Ludwigs, *Adv. Mater*. **2021**, *33*, 2007982.

[28] S. Bolte, F. P. Cordelières*, J. Microsc*. **2006**, *224*, 213.

[29] S. Huth, S. Sindt, C. Selhuber-Unkel, *PloS One*. **2019**, 14, e0220281.

Supporting Information

Increasing the Efficiency of Thermoresponsive Actuation at the Microscale by Direct Laser Writing of pNIPAM

*Tobias Spratte, Sophie Geiger, Federico Colombo, Ankit Mishra, Mohammadreza Taale, Li-Yun Hsu, Eva Blasco, Christine Selhuber-Unkel**

T. Spratte, S. Geiger, Dr. F. Colombo, A. Mishra, Prof. C. Selhuber-Unkel
Institute for Molecular Systems Engineering (IMSE), Heidelberg University, 69120 Heidelberg, Germany
E-Mail: selhuber@uni-heidelberg.de

L.-Y. Hsu, Prof. Dr. E. Blasco
Organic Chemistry Institute and Center for Advanced Materials, Heidelberg University, 69120 Heidelberg, Germany

Reversible shrinking and reswelling of pNIPAM hydrogel microstructures

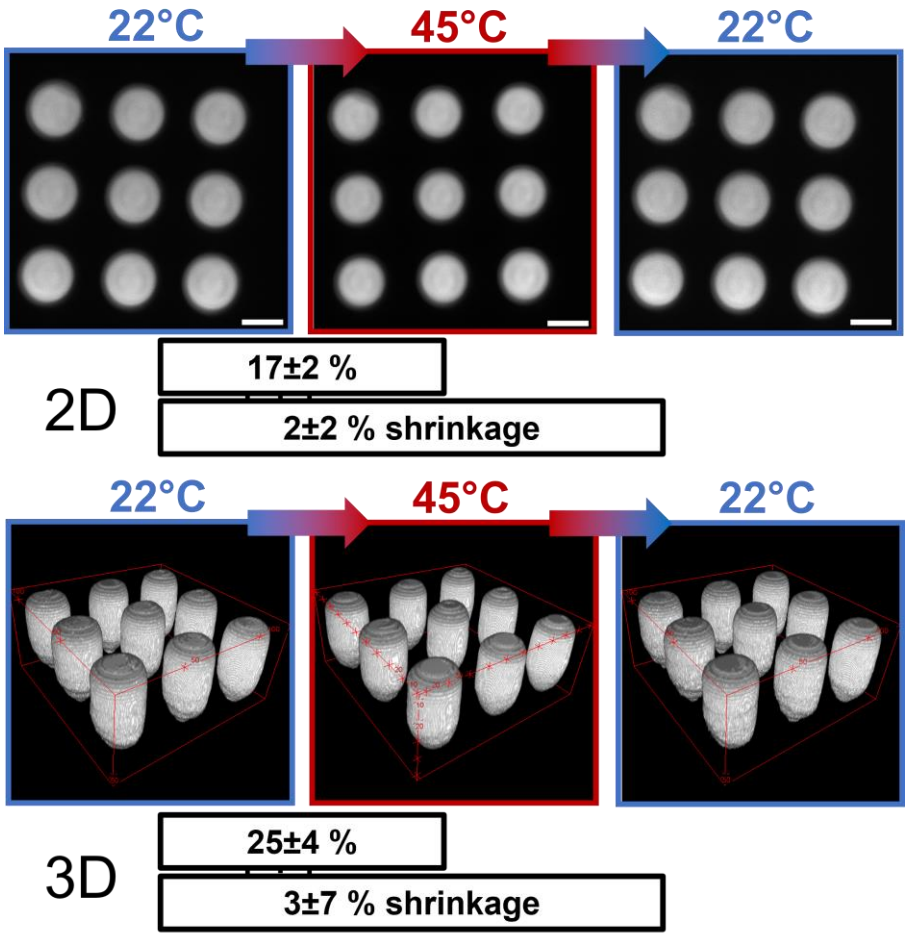

Figure S1. Reversibility of the thermally induced shrinkage of the 20 µm pNIPAM hydrogel microstructures. The micropillars were first measured at 22 °C, then heated to 45 °C and left to cool down to 22 °C again. Depicted are confocal fluorescence images of cross-sections and 3D reconstructions of the image stacks. Scale bars are 20 µm.

Correlation between writing speed, crosslinking degree and shrinkage

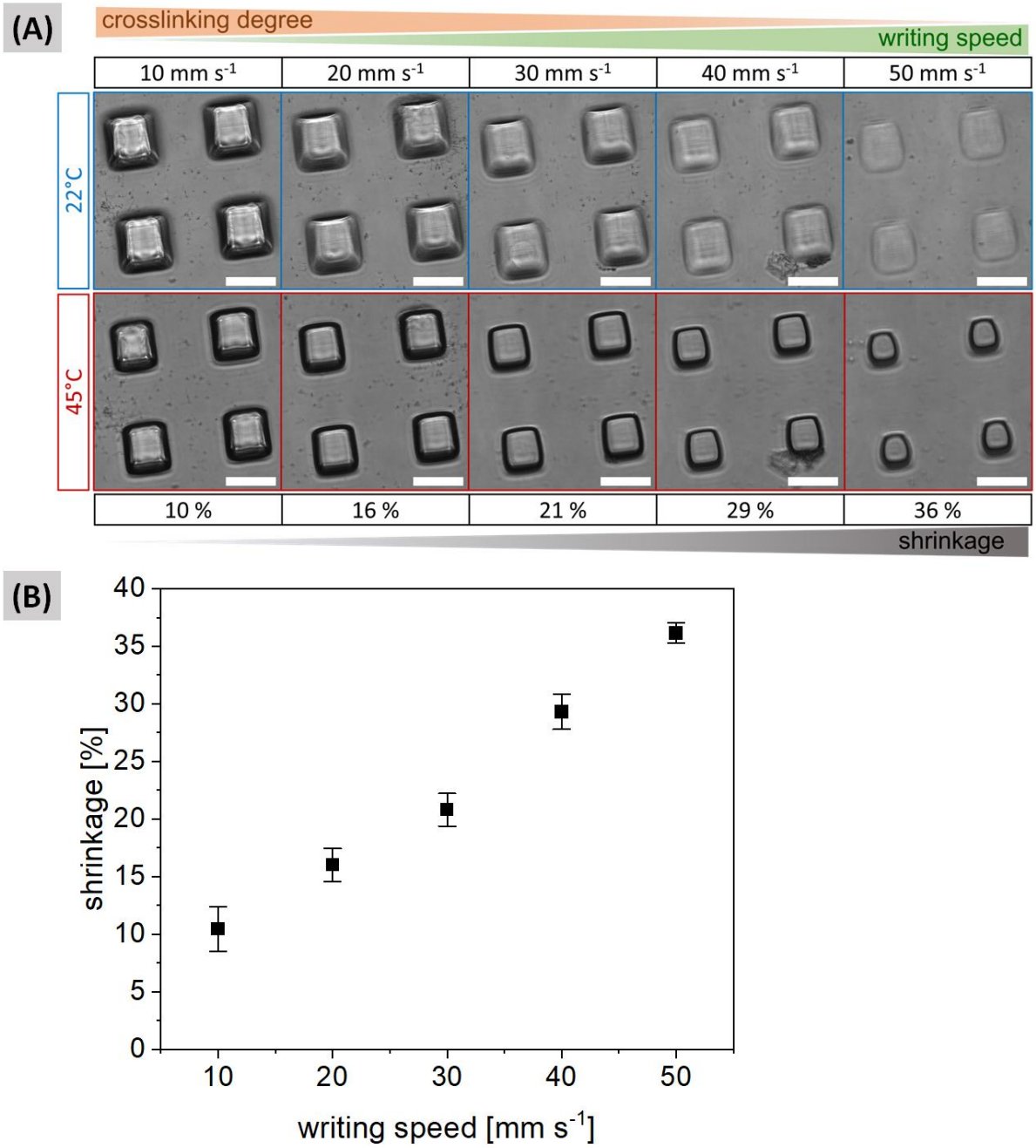

Figure S2. (A) Correlation of DLW writing speed, relative crosslinking degree and thermally induced shrinkage of pNIPAM hydrogel microcubes. An increase in writing speed causes a decrease in crosslinking degree and an increase in shrinkage (relative to the diagonal of the square cross section of microcubes). Scale bars are 50 µm. (B) The percentual shrinkage as a function of writing speed shows a linear correlation in the range of 10 to 50 mm s^{-1} (N=7).

Table S3. Comparison of pNIPAM soft actuator properties in other recent studies

Type of actuator	Response	Response time	Size	Reference
Thermally-driven microvalves	Opening and closing of valve structure	few minutes*	60 µm	this work
Light-driven microgripper	Closing and opening of a double-arm structure	33 ms	26 µm	[S1]
Light-driven microgripper	Closing of two arms	2 s	80 µm	[S2]
pH-responsive microrings	Blocking of microfluidic channel	200 ms	5-15µm	[S3]
Thermally-driven microbeams	Bending of beams	100 ms	30-120 µm	[S4]

* limited by heating / cooling rate

[S1] C. Zheng, F. Jin, Y. Zhao, M. Zheng, J. Liu, X. Dong, Z. Xiong, Y. Xia, X. Duan, *Sensors Actuators, B Chem*. **2020**, *304*, 127345.

[S2] L. Chen, Y. Dong, C.-Y. Tang, L. Zhong, W.-C. Law, G. C. P. Tsui, Y. Yang, X. Xie, *ACS Appl. Mater. Interfaces.* **2019**, *11*, 19541.

[S3] K. Hu, L. Yang, D. Jin, J. Li, S. Ji, C. Xin, Y. Hu, D. Wu, L. Zhang, J. Chua, *Lab Chip*, **2019**, *19*, 3988.

[S4] M. Hippler, E. Blasco, J. Qu, M. Tanaka, C. Barner-Kowollik, M. Wegener, M. Bastmeyer, *Nat. Commun.* **2019***, 10*, 232.